Available online at www.sciencedirect.com

ScienceDirect

Focus Article, *Mendeleev Commun.*, 2022, **32**, 143–151

Mendeleev Communications

Transition metal atoms grafted on the nanodiamonds surface: identification and guest–host spin–spin interactions

Ilya D. Gridnev*[a] and Vladimir Yu. Osipov[b]

[a] *N. D. Zelinsky Institute of Organic Chemistry, Russian Academy of Sciences, 119991 Moscow, Russian Federation. E-mail: ilyaiochem@gmail.com*

[b] *Ioffe Institute, 194021 St. Petersburg, Russian Federation. E-mail: osipov@mail.ioffe.ru*

DOI: 10.1016/j.mencom.2022.03.001

This survey describes recent achievements in creating a new type of materials – nanodiamonds grafted with atoms of transition metals. Structural features of some selected chelate complexes studied by density functional theory, their scope and limitations as well as possible applications are discussed. Using the example of copper ions, their location relative to subsurface defects of detonation diamond is investigated by the method of electron paramagnetic resonance (EPR).

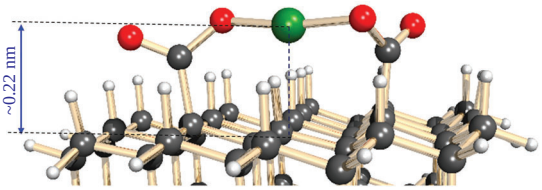

Scheme of a copper chelate complex on the 111 surface of a diamond. Atoms: black – carbon, red – oxygen, green – copper, white – hydrogen.

Keywords: nanodiamonds, 3*d*/4*f*-metals, chelate complexes, density functional theory, magnetochemistry, electron paramagnetic resonance.

Introduction

Detonation nanodiamond (DND) is a material consisting of particles with approximately 5 nm in diameter which are built from carbon atoms arranged in a diamond-like manner, ideally having a cuboctahedron shape and eight regular 111-surfaces[1] (Figure 1). This material is readily available from detonation of explosives during the utilization of out-of-dated weapons (so-called conventional DNDs synthesized from a mixture of trinitrotoluene–hexogen of composition 60 : 40).[2] Technologically, this is achieved by detonating 1–2 kg of an explosive charge in a closed volume (1–4 m^3) under conditions of negative oxygen balance and cooling the reaction products by pre-filling the chamber with carbon dioxide, or by forming a thick water armor around the charge.[3] The non-diamond phase is then chemically removed from the resulting batch, and the gray diamond phase is isolated. Under industrial conditions, DND particles are additionally treated in aqueous nitric acid at temperatures above 210 °C to remove sp^2 carbon shell from the surface of the particles. In this case, the color of the powder becomes even lighter.

DND particles are characterized by a high concentration of spin radicals, more than 1200 ppm (or 6×10^{19} spin per gram).

Ilya D. Gridnev received his PhD in 1989 from Moscow University. In 1990–1998 he was employed by Russian Academy of Sciences (Institute of Organic Chemistry and Institute of Organoelement Compounds). After two postdoctoral stays in Japan (JSPS Fellowship, Hokkaido University) and Germany (A. v. Humboldt Fellowship, Göttingen University) he got his Dr. Sci. Degree ('Habilitation') from A. N. Nesmeyanov Institute of Organoelement Compounds, Moscow, Russia. In 1998–2007 he was employed as a Research Associate in University of Rennes, France, Chiba University, Japan, and Oxford University, UK. In 2003–2007 and in 2012–2021 he was Associate Professor in Tohoku University (Sendai, Japan), and in 2007–2012 in Tokyo Institute of Technology. In 2021 he returned to Russia to take the position of a Leading Researcher in N. D. Zelinsky Institute of Organic Chemistry. His research interests cover asymmetric catalysis, computational chemistry, organometallic chemistry, reaction mechanisms, and NMR spectroscopy.

Vladimir Yu. Osipov received the degree of Electrical Engineer in the field of 'Optoelectronics and Optoelectronic Devices' in 1987 from St. Petersburg Electrotechnical University 'LETI'. He joined the Ioffe Physical-Technical Institute, Russia in 1987 as researcher and received his PhD on the speciality 'Semiconductor and Dielectric Physics' in 1994. He was appointed as Senior Scientist in 1999. He started to study detonation nanodiamonds and defects in diamonds in 1998 in close cooperation with collaborators from Katholieke Universiteit Leuven (Belgium). He was a visiting Associate Professor (2002) and JSPS Fellow (2004–2005) in Tokyo Institute of Technology and also occupied a position of JSPS Fellow in Hosei University (Tokyo, Japan) during 2017–2018. He was an invited Professor (2019) at ENS Paris–Saclay (France) where he delivered a course of lectures on the topic 'Paramagnetic defects in solids and carbon-based substances'. He is also a foreign scientific expert at Anhui University in Hefei (Anhui Province, China) since 2020. His current research interests include magnetic, electron spin resonance and optical properties of transition metal impurities and color centers in diamonds, and some issues of edge state paramagnetism in nanographites.

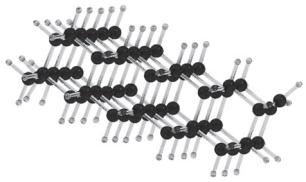

Figure 1 Model of a portion of a DND particle containing 70 carbon atoms.

Following ref. 4, this can be explained by the features of the detonation synthesis of diamonds under conditions of negative oxygen balance. These features are as follows.[5,6] When about 1 kg of a charge consisting of an alloy of trinitrotoluene–hexogen (60 : 40) is blown up in a closed volume, the released energy is not sufficient to completely atomize the molecules of the mixture, but they decompose into many molecular fragments, including radicals $CH_3^{\bullet}$, $CH_2^{\bullet\bullet}$, $CH^{\bullet\bullet\bullet}$, *i.e*. methane derivatives, and low-molecular gaseous detonation products formed during the development of the process and assembly of nanodiamonds: H^+, H^-, $H^{\bullet}$, N_2, H_2, CO, CO_2, NH_3, H_2O, N_xO_y.[5] Diamond particles are synthesized in the area of the detonated charge during the time when the shockwave passes the charge of 8–10 cm in size. The detonation velocity in this case is about 7 km s^{-1}, and the decomposition of the explosive molecules occurs in the front of the shock wave. Chemical reactions and product assemblies proceed in the corresponding local subregions after the shock wave front has passed through them. Under conditions of negative oxygen balance, this area during the first 10–14 μs of the process is a partially ionized gas (plasma) with free hydrocarbon and methyl radicals. In the chemical reaction zone following the moving front of the shock wave, the pressure reaches 20–21 GPa. The growth of diamonds slows down and stops at the stage of significant expansion of detonation products as a result of a sharp drop in pressure and temperature. To reduce the role of secondary shock waves reflected from the walls of the stainless steel chamber and to increase the yield of the diamond nanoscale phase, the charge is surrounded by massive water armor. Rapid assembly of diamonds is carried out from $CH_3^{\bullet}$, $CH_2^{\bullet\bullet}$ radicals according to a chemical mechanism similar to the process of growth of diamond and diamond-like films at low pressure (30–150 Torr) from a 1% methane in hydrogen gas mixture. The exceptionally high growth rate of diamond particles during detonation, due to the high temperature and high concentration of $CH_3^{\bullet}$, $CH_2^{\bullet\bullet}$ radicals in the detonation zone in the first 10 μs, leads to the fact that the assembly of diamond lattices in individual particles occurs with errors, with the formation of different point and collective defects, such as vacancies, built-in interstitial and substitutional nitrogens, dangling C–C bonds and twin boundaries.[4] In this case, during the first ~500 ns after the passage of the detonation front, 5–8 nm crystallites enriched by defects and primary clusters based on them are formed.[7] As the gaseous products are unloaded and expanded from the zone where the detonating charge is located, the synthesis of diamond nanoparticles stops. As a result, the powder product isolated after removal of the non-diamond sp^2-phase has an enormous (compared to bulk microcrystals) amount of paramagnetic centers with spin 1/2. These spins are localized within the diamond crystallites and distributed in them with predominant localization in the outer defect layer up to 1–1.3 nm thick.[4] The prevalence of spin radicals in the outer layers is due to the fact that the outer layers of 5 nm diamond particles are formed almost at the final stages of the process, during such an expansion of the detonation products, when the pressure in the plasma drops and the composition of the gaseous detonation products changes greatly. An alternative, but less developed, model of DND formation from liquid carbon droplets formed during detonation can also explain the high concentration of spins in the outer layers of DND particles. This property makes it possible to use DND spin-radicals as an extremely stable, for decades, standard with a fixed high concentration of spins 1/2, which can be used for metrological purposes. For the first time, the main paramagnetic properties of DNDs were described in detail in ref. 8, which has by now more than one and a half hundred citations.

In fact, real DND particles contain a certain number of surface functional groups (OH, COOH, *etc*.) which can be used for the chemical modification of their surface leading to various practically applicable molecules.[9–12]

Moreover, fixation of various transition metals on the surface of nanodiamonds provides a new type of smart materials with numerous already developed and perspective applications.[13–15]

Incorporation of Cu atoms on the surface of nanodiamonds is usually accomplished by mixing the water suspension of acid-purified DNDs (0.12–0.5 wt%) and water solution of copper-containing salt (acetate or nitrate) followed by isolation of the sedimented solid part and its heating and drying.[16,17] Therefore, it is interesting to follow the chemical processes taking place during this procedure by means of quantum-mechanics computations and methods of magnetic diagnostics of 3*d* and 4*f* metal ions.

In this work, we analyze the theoretical aspects of the formation of metal complexes on the DND surface and consider the latest experimental results on the fixation of some transition metal ions on the surface of DND particles.

Computational studies of the nanodiamonds grafted with copper

Computational studies of the nanodiamonds grafted by transition metals is a relatively new area. On the early stages of fabrication and studies of these materials it has been suggested that the metal ions are held on the particles surface by purely Colombian forces. However, this suggestion is counterproductive from two different points of view. First, it leaves behind the chemical reactions ultimately leading to the formation of such particles. Second, it cannot adequately describe the final species with the metallic atoms firmly incorporated into the body of the nanoparticle where the metal and surrounding atoms are definitely bound by normal chemical bonds.

Having these considerations in mind, unrestricted DFT computations on the B3LYP/6-31G* level of theory either in water (IEFPCM) or in a gas phase using Gaussian09 software were carried out. The use of the hybrid DFT theory is the most efficient and accurate computational method for the description of coordination compounds including copper complexes.[18–20]

Computations showed that formation of a non-chelating complex with copper acetate is possible and exothermic (17 kcal mol^{-1}). However, it was concluded that the copper atoms incorporated in that way are likely to be lost during the thermal treatment, because otherwise much more copper atoms could be positioned on the surface than is experimentally observed. Hence, the formation of chelating complexes was examined in more detail.

Analysis of the geometries of the relative positions of carboxyl groups on the 111-surface allowing for the formation of a chelate complexes revealed two possibilities (Scheme 1).

Reaction of copper acetate with two carboxyl groups of **1** yields exothermically the adduct **3**. Further, a real surface chelate complex **4** with two coordinated molecules of acetic acid is produced (Scheme 2). This brings the Cu atom 0.052 nm closer to the surface, but the Cu–O bonds are only slightly shorter in **4** than in **3** (Table 1). Removal of the acetic acid molecules from **4** *via* after-treatment of the Cu-doped nanodiamonds (in the secondary vacuum) yields **5**, in which structure of the chelate

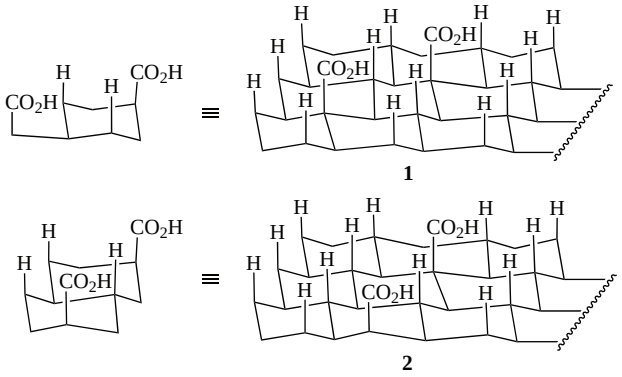

Scheme 1 Two possible arrangements of the pair of carboxylic groups on the surface of nanodiamond that could bind copper ion in a chelate manner.

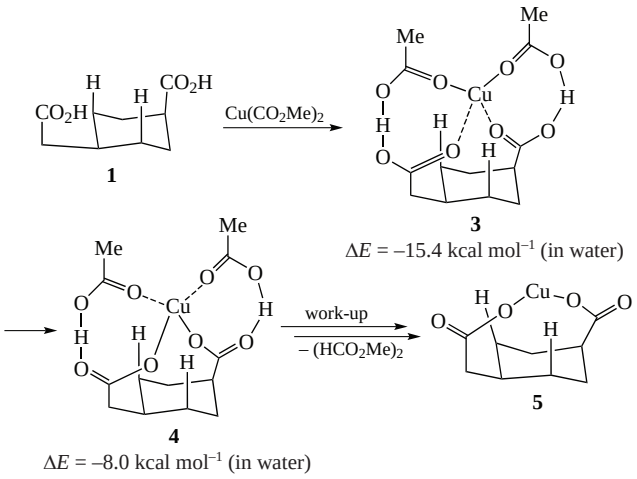

Scheme 2 Formation of the chelate complex **5**. All energies are given respective to **1** + $Cu(CO_2Me)_2$. Here Me = CH_3 (methyl group).

Table 1 Selected parameters of copper chelate complexes on the diamond surface.[a]

Compound	Bond Cu–O(1) length/nm	Bond Cu–O(2) length/nm	Relative energy/ kcal mol^{-1}	Distance to the surface/nm
3	0.196	0.196	–	0.373
4	0.192	0.190	–	0.321
5	0.176	0.176	0	0.282
6	0.176	0.180	11.1	0.227
7	0.178	0.178	–14.8	0.225
8	0.178	0.179	–20.5	0.222
9	0.176	0.176	2.4	0.287
10	0.179	0.179	5.6	0.221
11	0.181	0.179	–7.1	0.230

[a] All energies are given relative to **5**.

complex changes dramatically *via* shortening of the Cu–O bonds and flattening the O–Cu–O angle that brings the Cu atom as close as 0.282 nm to the surface. This trend is still more evident in the gas phase (see Table 1).

Figure 2 shows the chelate complex **5** together with other optimized structures **6**–**8** of different Cu chelates formed on the nanodiamond surface. Relative energies of different species demonstrate the preference for formation of the clusters at the edges of the nanoparticle.

Although formation of the chelates in the case of the spatial arrangement of the carboxylic groups by type **2** of diamond surface piece intuitively seems less favorable, quite stable structures **9**–**11** were located with the geometry of the O–Cu–O fragment and its closeness to the surface quite similar to those

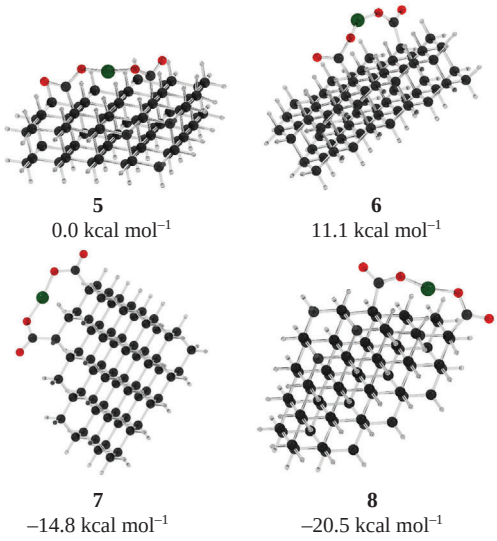

Figure 2 Optimized structures and relative energies of four chelate Cu complexes built using the arrangement of two carboxyl groups of type **1**.

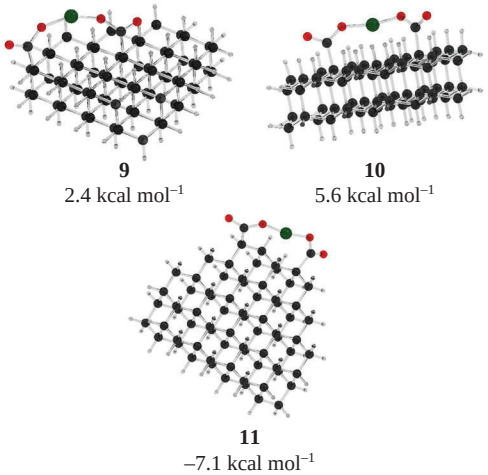

Figure 3 Optimized structure and relative energies of three chelate Cu complexes built using the arrangement of two carboxyl groups of type **2**.

seen in **5**. It was concluded that formation of both structures is equally possible, although the hindrance from the nearby C–H bond (the distance between the copper atom and the closest proton in **9** is 0.184 nm) may prevent the formation of **9** kinetically. The structures of compound **9** and similar complexes of the type **2** are shown in Figure 3.

Similarly to the chelates appeared on the diamond surface pieces of type **1**, the relative stability of compounds **9**–**11** increases with the approach to the edge of the nanoparticle.

A possibility of a radical defect in the location that is occupied by the hindering C–H bond in **2** was considered (Scheme 3). A structure **12** with very short distance between the copper atom and the surface of the nanodiamond (0.197 nm) has been found (Figure 4). Compound **12** is formed by oxidation of Cu^{II} to Cu^{III} that is accompanied with the formation of a Cu−C bond. In the ground state **12** is a singlet, hence it is silent in the EPR spectra. The triplet state of **12** is 40 kcal mol^{-1} higher in energy.

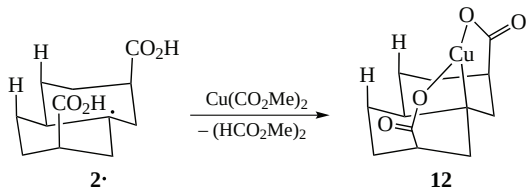

Scheme 3 Formation of the singlet complex of Cu^{III} **12**.

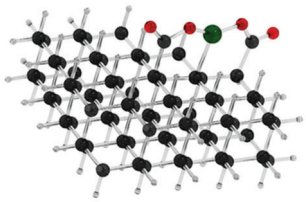

Figure 4 Optimized structure of chelate Cu^{III} complex **12**.

Several structures containing heteroatoms were also computed. As could be expected, such heteroatoms strongly affect the structures of the resulting chelate complexes, leading sometimes to rearrangements, that however do not affect the possibility of the fixation of copper atoms on the surface. Rather, these results suggest further opportunities of the modification of nanodiamond particles.[21]

Computations were also applied for estimation of the maximal number of copper atoms that can be grafted on the surface of a nanodiamond particle.[22] Suggesting that all appropriate positions are occupied with the carboxyl or hydroxy groups that bind copper atoms, estimation of 34 wt% per nanoparticle has been obtained.[22] In practical terms, the loading of particles with such a number of copper atoms in a bound form is not feasible when using the methods of wet chemistry. Let us consider below the realistic situations that arise when using wet chemistry for chelating the DND surface with metal complexes.

Recent experimental studies of transition metals grafted on the DND surface

Gadolinum complexes on the carboxylated surface

In addition to copper, other 3*d* transition metals also form chelate complexes on the DND surface in the form of doubly charged ions trapped by carboxy groups. These include nickel, cobalt and iron. In turn, the 4*f* transition metals also form chelate complexes on the DND surface. Among them are gadolinium, terbium, holmium, and europium. The interaction of surface carboxyl groups with triply charged ions of some lanthanides, leading to controlled formation of complexes, was recently studied by physicochemical methods in ref. 23. The scheme of the ion exchange reaction in a mixture of saline solution and DND suspension, leading to the formation of gadolinium chelate complexes, is shown for example in Figure 5(*a*). At the same time, in an aqueous medium, carboxyl groups on the DND surface are dissociated. Three-charged ions of 4*f* transition metals can be fixed on the diamond surface through triads of specially arranged carboxyl groups located at the nodes of the diamond lattice, forming a regular triangle. One such configuration with a gadolinium chelate complex is shown in Figure 5(*b*). The gadolinium ion is centered between these carboxy groups, and is approximately the same distance from the diamond surface (0.32 nm) as the copper ion in the chelate complex of two carboxy groups (~0.25 nm).[24]

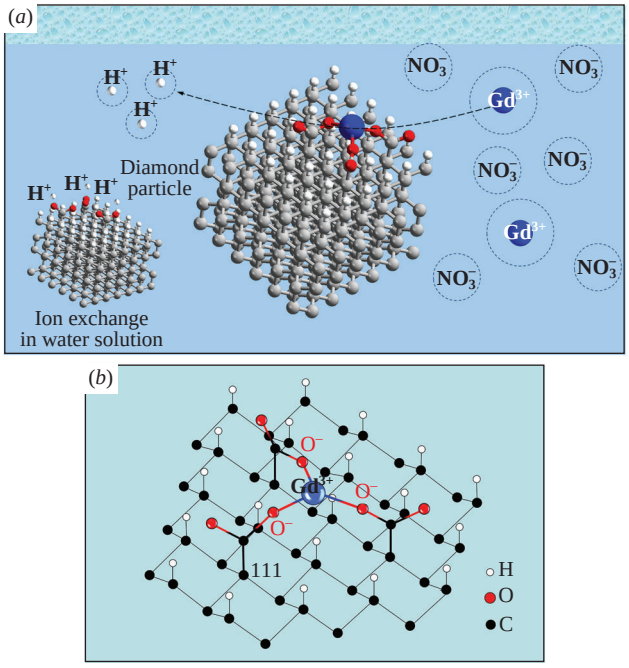

Figure 5 (*a*) Scheme of the ion exchange reaction in a mixture of an aqueous solution of gadolinium nitrate and an aqueous suspension of 5 nm DND particles and (*b*) the sketch of Gd^{3+} ions fixation on the functionalized (111) diamond surface *via* the triads of neighboring deprotonated carboxyl groups. Panel (*a*): solvation shells around cations and anions are shown schematically. Atoms: carbon – gray, oxygen – red, hydrogen – white, gadolinium – blue. Panel (*b*): for simplicity, the diamond surface is saturated with atomic hydrogen, and the water molecules that additionally coordinate the gadolinium ion in the complex are not shown.

It should be noted that chelate complexes of 3*d*- and 4*f*-metals are formed on the surface of only carboxylated nanodiamonds, whose surface was preliminary oxidized by heating in air in the temperature range 420–520 °C. For nanodiamonds treated in a hydrogen atmosphere or hydrogen plasma, with a surface saturated with atomic hydrogen or hydroxyl groups, such a non-chemical adsorption of metal cations is observed when the corresponding solutions are mixed, although the DND suspension with a positive zeta potential is stable.

The infrared absorption spectra of DND with a surface most suitable for the formation of chelate complexes are shown in Figure 6 by red lines. The spectra shown in Figure 6 differ in the temperature of DND treatment in air and indicate the presence of a large number of C–O, C–O–C bonds on the particle surface as well as carbonyl groups C=O and groups OH. The extended absorption band in the range 900–1500 cm^{-1} is due to the presence of C–O, C–O–C and OH groups in the DND molecular shell. The absorption bands from the indicated groups overlap strongly in this region and are practically indistinguishable. A relatively narrow absorption band centered at 1790 cm^{-1} (spectra *2*, *3*) is associated with vibrations of C=O groups, and the band at 1630 cm^{-1} of the same width is associated with vibrations of hydroxyl groups. Here we believe that the registered carbonyl groups are part of the carboxyl groups as constituent elements. Therefore, the presence of a pronounced band at 1790 cm^{-1} is evidence of the presence of a carboxylated diamond surface, with a vanishingly small fraction of the surface terminated by atomic hydrogen. DNDs with such a surface are formed from factory DND purified in acids after treatment in air at a temperature of 430 °C and even higher (up to 520 °C).[25] In

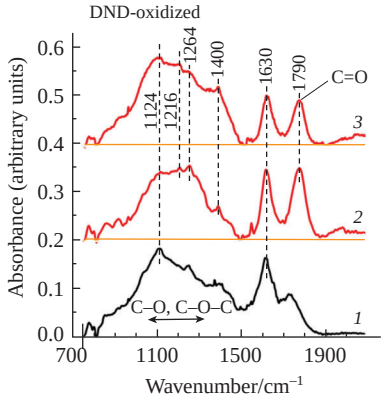

Figure 6 IR absorption spectra of detonation diamond powders thermally treated in air. Processing temperature, °C: *1* – 350, *2* – 430, *3* – 520. For clarity, spectra *2* and *3* are shifted in the vertical direction by 0.2 and 0.4 scale units, respectively. The absorption bands associated with carbonyl C=O groups are clearly visible in spectra *2* and *3* at 1790 cm^{-1}.

the case of processing at 350 °C, the surface is still insufficiently oxidized and does not contain a sufficient amount of carboxyl groups required for chelation of metals. This is clearly seen from the intensity of the ~1740 cm^{-1} band from C=O groups in spectrum *1* (black line, Figure 6). The latter is shifted by 50 cm^{-1} towards lower vibration frequencies and has a small amplitude compared to the band at ~1630 cm^{-1}.

Magnetic studies carried out at low temperatures showed that gadolinium ions form chelate complexes on the DND surface in a wide concentration range, from 1.53×10^{18} to 7.85×10^{19} g^{-1}. The data were obtained by analyzing the magnetization curves of the samples in the saturation mode of magnetization in fields greater than 3 T, with an estimate of the concentration of sites carrying a spin of 7/2 corresponding to the spin of the gadolinium ion [Xe]$4f^7$ [Figure 7(*a*)]. Spins with lower values were not found on the surface of DND particles.

These estimates were made based on the plotted magnetization curves related to the subsystem of gadolinium ions on the DND surface.[24] Determining the magnetization from only gadolinium ions (or lanthanides with large magnetic moments) is not entirely trivial in terms of the procedure and required accurately estimated deductions from the magnetization of the sample of other contributions, namely, from the diamagnetic crystal lattice of diamond and the ensemble of paramagnetic spins 1/2 present in diamond particles.[24,26]

The highest achieved concentration (7.85×10^{19} g^{-1}) of gadolinium ions in the powder of DND particles corresponds to approximately 18 metal ions on the surface of a 5-nm DND particle. The same data on the amount of gadolinium ions on the DND surface can be obtained from the analysis of the temperature dependence of the magnetic susceptibility (χ) of the DND-Gd samples synthesized in ref. 24. All samples with different contents of gadolinium demonstrate the Curie character of the magnetic susceptibility according to the formula

$$\chi_{Gd} = C/(T - \theta).$$

Here C is the Curie constant associated with the spin subsystem of gadolinium ions and θ is the Weiss temperature. Here, by χ_{Gd} we mean the purely magnetic susceptibility of the gadolinium ion subsystem, which is one of the components in the susceptibility of the DND-Gd system according to the formula

$$\chi = \chi_{Gd} + \chi_{PC} + \chi_{dia}.$$

Here, the second and third terms in the formula are related to the paramagnetism of spins 1/2 inside diamond particles and the weak diamagnetism of the diamond lattice. Figure 7(*b*) shows the dependences of the $\chi_{Gd}T$ product on T for all studied DND-Gd samples in the temperature range of 2–300 K. The numbers near the curves correspond to the concentration of Gd^{3+} ions determined by this method (from Curie constants). These values in g^{-1} units are in good agreement with the values indicated in Figure 7(*a*). A slight downward turn at $T < 10$ K for all curves shown in Figure 7(*b*) is associated with a nonzero Weiss temperature, which for all samples is about –0.7 K and indicates a weak antiferromagnetic interaction of atomic spins 7/2.

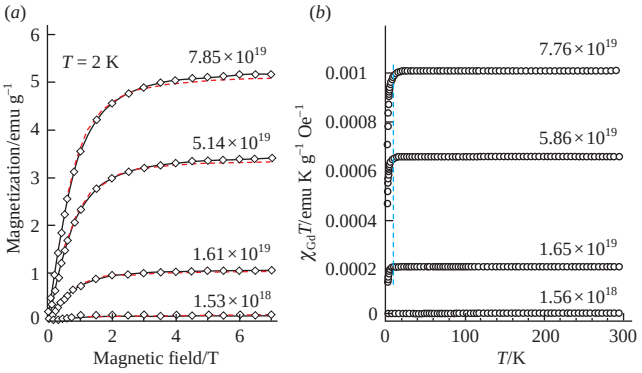

Figure 7 (*a*) M–H magnetization curves taken at $T = 2$ K and (*b*) temperature dependences of the $\chi_{Gd}T$ value taken in the field $H = 0.8$ T for ensembles of isolated Gd^{3+} ions on the surface of DND particles, for different metal contents in the powder. The contribution from the intrinsic magnetization of the diamond matrix (unmodified DND) is subtracted and is not shown in the M–H graphs. The red dashed lines in panel (*a*) show the fitting curves constructed using the Brillouin formula for the spins $S = 7/2$ and the Gd^{3+} spin concentrations indicated on the curves in units of g^{-1}.

Although isolated DND particles with so many 4*f* ions with a large magnetic moment do not possess superparamagnetic properties due to the almost zero magnetic interaction of atomic spins $S = 7/2$, they are extremely promising as contrast enhancers in magnetic resonance imaging (MRI).[14,27,28] The latter is especially important in connection with the permeability of cell membranes for particles of this size. It is known that the MRI method gives the distribution of water density in biological tissues, due to which the morphology of tissues is well visualized. The local signal itself at a given point of the object is associated with the relaxation time of the magnetic moments of the water protons. Molecular agents with high magnetic moments used to decorate biological tissues enhance the water proton relaxivity and increase the visualization contrast. DND particles with grafted gadolinium ions give much better results than well-known MRI contrast enhancers such as Gd-DTPA ($C_{14}H_{18}GdN_3O_{10}$) and Gd-BOPTA ($C_{22}H_{28}GdN_3O_{11}$) and many others.[14] It is believed that Gd-grafted DND particles are a potentially safe contrast agent for *in vivo* MRI and clinical applications. This is because the latter can be additionally coated with a thin layer of polyvinylpyrrolidone.[28] This coating prevents particle aggregation in the saline environment and prevents vascular blockage.

Copper complexes and their location

Interest in the fixation of copper on the surface of DND particles through chelate complexes is due to the fact that, of all 3*d* transition metals, bivalent copper ions are well diagnosed by the EPR method.[29,30] Copper is well recognized in EPR spectra by unique signatures associated with the hyperfine interaction of the magnetic moments of the Cu^{63} and Cu^{65} nuclei with the electron spin Cu^{2+}. As a result, not only acetates, but also copper nitrates can be used for the chelation reaction. In our recent work, the modification of a single-particle suspension of DNDs with ionic copper was described in detail, and isolated materials with different copper contents (from 1 to 2.3 wt%) were studied by the EPR method.[31] Below these results are discussed in more detail.

X-band electron paramagnetic resonance (EPR)

As an example, consider the EPR spectrum and its components for one specially prepared dry sample NDCu-ii modified by copper in amount no less than 1.5 wt%. The EPR spectrum of this sample is presented in Figure 8(*a*),(*b*) both in normal and in integral representation (after single integration of the experimentally measured spectrum with respect to the variable magnetic field). More precisely, Figure 8(*b*) shows the total consolidated EPR signal from all types of spins obtained after numerical integration of the primary signal of the first derivative of absorption (dA/dH) in a wide range of magnetic fields from 2350 to 4350 G. A flat even background in the regions <2500 G and >3650 G allows one to well determine the base zero level and thereby separate the signals from the DND carbon matrix proper and copper ions, and metrologically accurately estimate the contribution to the total signal from copper ions per unit mass

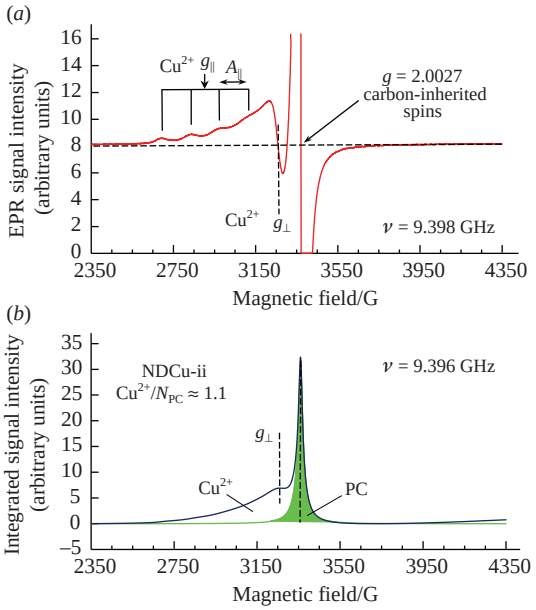

Figure 8 (*a*) EPR spectrum of sample NDCu-ii just after recording and (*b*) the same one after integration over the variable H (magnetic field) in the range 2350–4350 G, showing contributions from Cu^{2+} ions (open area) and the DND matrix itself (shaded in green). T = 293 K. Microwave frequency – 9.397 ± 0.001 GHz.

of carbon or the total number of spins in the diamond matrix. On the integrated EPR spectrum in Figure 8(*b*), a relatively narrow EPR signal from the DND is specially highlighted in green. It is a superposition of two Lorentzian contours of different widths. It is easily identified due to the large amplitude of the resulting signal with g = 2.0027 from defects in the diamond matrix. From the integrated EPR spectrum of DND-Cu in Figure 8(*b*), it can be seen that the contributions to the integrated intensity of the EPR signal from Cu^{2+} spins 1/2 and spins 1/2 of the diamond matrix are approximately the same. To determine the proportion of the former accurately, it is necessary to subtract the EPR signal of the diamond matrix from the total consolidated signal. Subtraction of the narrow DND EPR signal (two Lorentzian contours *L*1, *L*2) from the integral spectrum precisely determined the EPR signal from Cu^{2+} in the integral representation. Difference EPR spectra of bivalent copper ions for DND-Cu samples (labeled as NDCu-i, NDCu-ii and NDCu-iii) with various Cu content are shown in Figure 9 in integral representation. Each of them was obtained by direct subtraction

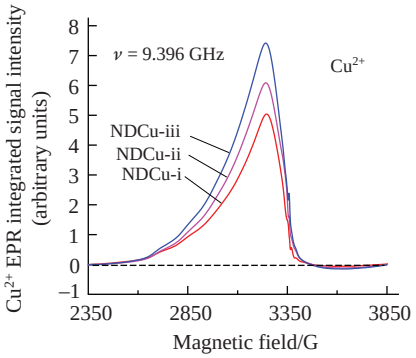

Figure 9 Integral, obtained after mathematical processing, EPR spectra of Cu^{2+} ions adsorbed on DND particles for samples NDCu-i, NDCu-ii and NDCu-iii. Microwave frequency: 9.396 GHz. Temperature T = 293 K. Before processing, the original spectra were recorded with the following parameters: microwave power – 2 mW, magnetic field modulation – 1 G, single spectrum recording time 90 s, number of signal accumulations – 6. The subtracted EPR signal from the diamond matrix was represented as the sum of two Lorentzian contours of different widths with approximately the same *g*-factors.

of the EPR signal of the diamond matrix from the integral EPR spectrum of the corresponding sample. Noteworthy is the feature at H = 3360.7 G. It is located at the edge of the descending high-field slope of the spectrum and is possibly associated with some additional signal of unknown origin or an artifact of numerical processing. The latter is clearly seen in the direct differentiation of the integral EPR spectra of DND-Cu series. The *g*-factor of this signal is 2.0030 (after correcting the magnetic field values by ~8 G downward when using a powder EPR standard). The spectra in Figure 9 are not reduced to the unit weight of the powders, but are normalized to the total number of 1/2 spins (N_{PC}) in the diamond matrix, *i.e.* on the intensity of the narrow main EPR signal with a *g*-factor of 2.0027 from a group of spins located in diamond particles. In control samples made on the basis of aqueous suspensions of DND from Adamas Nanotechnologies (US), the value of N_{PC} is about $\sim 7 \times 10^{19}$ spin per gram.

For these three spectra, the ratio of the numbers of spins in both spin groups $[Cu^{2+}]/N_{PC}$ varies from 0.91 to 1.34. As this ratio increases, the widths of the Lorentz contours *L*1 and *L*2 increase as shown in Figure 10. As can be seen from Figure 10, the broad Lorentzian component of the EPR signal (*L*2) is more sensitive to the amount of ionic copper on the surface. The reason for this is that the *L*2 component is caused by paramagnetic centers of shallow (< 0.8–0.9 nm) occurrence, and the narrow component *L*1 is caused by paramagnetic centers located deeper (> 0.9 nm). The broadening mechanism is a dipole–dipole interaction between the spins of both groups – copper spins and spins in a diamond lattice. The mean distance between a carbon-inherited spin and a Cu^{2+} 3*d*-shell spin was estimated at ~1.1 nm. Such an estimate was made in ref. 30, but the experimental data accumulated over the past decade for different DNDs require its refinement on the basis of a more advanced analysis. Following refs. 32, 33, the change in the EPR linewidth, depending on the concentration of the paramagnetic agent N_{Cu}, occurs in accordance with the formula:

$$\delta B_{pp} = \sqrt{(\Delta B^0_{pp})^2 + c(4\pi)^{-2} n_{Cu} g^2 \mu_0^2 \mu_B^2 S(S+1)\overline{d_{Cu}^{-6}}} - \Delta B^0_{pp} \approx$$
$$\approx \text{const} \times n_{Cu} \overline{d_{Cu}^{-6}}.$$

Here ΔB^0_{pp} is the width of the EPR line for DND with zero copper content, n_{Cu} is the ratio of the number of copper spins (N_{Cu}) to the number of intrinsic internal spins (N_{PC}) in DND particles, d_{Cu} is the mean distance between the shallow paramagnetic spin in DND particle and interior Cu^{2+} 3*d*-shell spin, and $\overline{d_{Cu}^{-6}}$ is the spatial average for the diamond lattice spin–copper spin distance in the rate –6 for all possible pairs of such spins belonging to one particle; $g \approx 2$ – *g*-factor for Cu^{2+} EPR signal, μ_B – Bohr magneton, $\mu_0 = 4\pi \times 10^{-7}$ H m^{-1} – magnetic constant, S = 1/2, $c = 4/15 \times 2.354^2 \approx 1.478$. Note that the formula is written in the

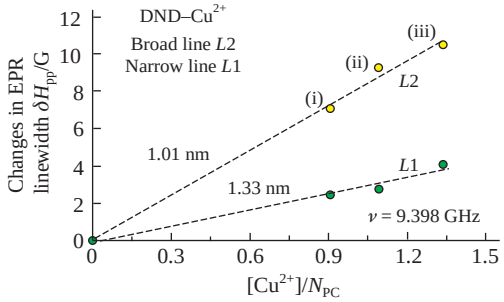

Figure 10 Changes in the width of the narrow (*L*1) and wide (*L*2) Lorentzian components of the main EPR signal (g = 2.0027) of the DND *versus* the relative content of paramagnetic copper on the particle surface. The linewidths for the narrow and wide components of the EPR spectrum at zero copper content are 8.7 and 17.2 Gauss, respectively.

SI system, where the quantities δB_{pp} and ΔB^0_{pp} are given in tesla units and $B = \mu_0 H$ in vacuum. The smaller the distance d_{Cu}, the greater the slope of this dependence of the EPR line broadening on the concentration of Cu^{2+} spins $S = 1/2$. The lower curve from Figure 10 corresponds, therefore, to paramagnetic spins deeper in the diamond matrix. If we rely on the application of the above formula, which was first used to analyze the data on the broadening of the EPR line for another model system nanographite–molecular oxygen,[32] and compare those data with ours, we can conclude that the value of $d_{Cu} \approx 1/\sqrt[6]{d_{Cu}^{-6}}$ for shallow spins in our case is at least 1.01 nm, and is expected to be greater than 0.8 nm obtained in ref. 32 for physisorbed oxygen molecules. The corresponding depth of occurrence of shallow paramagnetic spins is 0.22–0.28 nm less than d_{Cu} and equal to ~0.76 nm. The indicated depth of shallow spins is quite reasonable, since it is *a priori* obvious that a diamond particle contains the largest number of defects and dangling bonds within a few lattice constants from the surface. The estimated distance d_{Cu} and the depth of occurrence of deeper paramagnetic spins in the DND are 1.33 and 1.08 nm, respectively. Our estimates of the depths of occurrence of paramagnetic centers in the DND (~0.76 and ~1.08 nm) are in good agreement with the depth interval (0.3–0.9 nm) obtained in ref. 34 by the method of proton spin-lattice relaxation of surface hydrogen atoms. This is especially true for shallow centers.

Let us note that only zirconium was found (in addition to natural impurities of nitrogen and oxygen) as a heavy foreign element in the DND precursor. Its presence is due to the use of grinding balls made of zirconium dioxide in the production technology of a 5-nm DND suspension and a small amount of their traces (micro-fragments) in the final product. Since the Zr^{4+}: $[Kr]5s^04d^0$ ions in stoichiometric ZrO_2 have zero magnetic moment, they should not affect the quality of the EPR spectra. Here we also neglect the influence of paramagnetic defects in pure zirconium dioxide, namely: Zr^{3+} ions, yielding an axial signal ($g_{||} = 1.958$ and $g_{\perp} = 1.979$) and oxygen monovacancies. No specific EPR signals with a *g*-factor $g < 2$ located in the high-field wing of the main EPR signal of the DND were found.

X-ray photoelectron spectroscopy

The survey XPS spectrum of sample ND-Cu 5-nm is shown in Figure 11(*a*) together with the fragments of the spectra of the peaks Cu2*p* and N1*s* for the same sample (panels *b*, *c*). The relatively large height of the O1*s* peak in the survey spectrum [Figure 11(*a*)] indicates a high concentration of oxygen-containing groups on the surface of 5-nm DNDs that can bind metal ions. After the addition of ionic copper, the intensity of the O1*s* peak in the XPS spectrum for ND-Cu practically does not change compared to that in precursor nanodiamonds, but new weak peaks appear in the spectrum at 930–960 eV associated with the Cu2*p* signal [Figure 11(*b*)]. This Cu2*p* signal is characterized by three lines at ~932.6, ~943, and ~952.7 eV. The side components $2p_{1/2}$ and $2p_{3/2}$ of the Cu2*p* peak are due to the spin–orbit splitting of the Cu2*p* level ($\Delta \approx 19.8$ eV).[35] Each of them is due to copper in the Cu^{1+} and Cu^{2+} states. This is clearly seen from the asymmetric shape of the $2p_{3/2}$ peak [Figure 11(*b*)]. The peak at ~943 eV is satellite and is mainly due to copper in the Cu^{2+} state.[36,37]

The high-energy wing (B.E. above 402 eV) of the N1*s* signal, extending along the energy scale by ~6 eV, as in the ref. 38, is associated with surface nitrogen-oxygen (NO_x) groups, and the main central peak (at ~400.5 eV) with impurity nitrogen atoms in the sp^3 covalent lattice of diamond. The core of this N1*s* signal at ~400.5 eV [Figure 11(*c*)] is mainly associated with isolated substitutional nitrogen, or dimers based on the nearest in the lattice neighboring nitrogen atoms NN. The concentration of such nitrogen in DND exceeds 2 at%. Similar results for nitrogen content were obtained for different types of DND and much earlier.[38,39] This is due to the fact that nitrogen is always incorporated into the diamond lattice at the stage of explosive synthesis and its source is the native nitrogen of the components of the explosive mixture hexogen–trinitrotoluene.[40] Substitutional nitrogen with spin 1/2 in the diamond lattice is partially responsible for the paramagnetic properties of DND and determines the presence (~2 ppm) of nitrogen-vacancy complexes with unique luminescent properties in the particles.[40] Data on the content of individual elements in sample DND-Cu with maximum copper content are given in Table 2. They were obtained from the analysis of the intensities of the peaks in the survey XPS spectrum of the NDCu-iii sample (according to the standard method).[41]

According to XPS, for heavy-doped sample NDCu-iii, the copper content is 0.47 at% or ~2.3 wt%. This corresponds to 54 copper atoms on one DND particle 5 nm in size. This is 1.5–1.6 times more than the value determined by the SEM-EDX method. At the same time, according to the EPR data, the $[Cu^{2+}]/N_{PC}$ ratio is 1.34. Since the concentration of PC in DND is ~1300 ppm, the number of Cu^{2+} ions in one DND particle of 5 nm in size is 20. Hence it follows that the amount of ionic

Table 2 Elemental composition of heavy-doped DND-Cu sample for the first five elements most prevalent in it.

Element and level	Content (at%)	Content (wt%)	ZrO_2-corrected content (wt%)
C1*s*	83.74	76.62	79.448
O1*s*	13.14	16.03	15.661
N1*s*	2.27	2.42	2.513
Cu2*p*	0.47	2.28	2.378
Zr3*d*	0.38	2.64	–
	100%	100%	100%

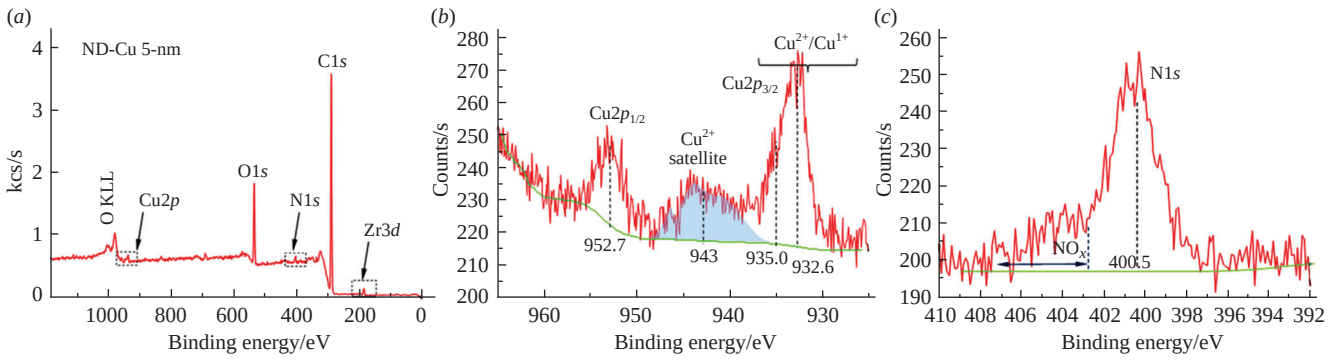

Figure 11 (*a*) The survey XPS spectrum of sample NDCu-iii together with detailed spectra of peaks (*b*) Cu2*p* and (*c*) N1*s* for sample NDCu-iii with maximum copper content (2.28 wt%).

bivalent copper on the DND surface is about 37% of the total number of deposited copper, or the XPS method overestimates these data for 1.5–1.6 times. It seems that at least 45% of copper is on the surface of DND particles in a non-paramagnetic state (in neutral clusters or in a +1 charge state).

At the same time, we should note that the XPS spectra of both the original DND-*ini* sample and doped D1–D3 contain Zr3*d* peaks at ~183–185 eV [Figure 11(*a*)]. The weight content of zirconium, estimated from the intensity of this peak, is ~2.64 wt% or 0.38 at% (for NDCu-iii). The fourth column of Table 2 shows the corrected data for the elemental composition of NDCu-iii as a result of subtracting the percentage of zirconium and oxygen in units of atomic percent. A strong argument confirming the correctness of all our quantitative XPS data is the almost identical presence of zirconium from the parasitic ZrO_2 phase in all samples, estimated from the area of the weak peak at 184 eV from the Zr3*d* level.

Energy dispersive X-ray analysis

Elemental composition information was also obtained by Energy Dispersive X-ray (EDX) analyzing the powder surface on a conductive substrate. Figure 12 shows the EDX spectrum of sample NDCu-iii from an area with a local copper content of 1.43 wt% (0.29 at%). The oxygen content is 9.38 at%. Possibly 0.48 at% of oxygen is part of zirconium oxide. This means that the content of atomic oxygen bound to the surface (about 8.9 at%) is approximately 30 times higher than the amount of atomic copper. It can be assumed that the number of copper atoms on the surface is only 7.5 times less than the number of pairs of carboxyl groups chelating doubly charged cations. According to the maximum estimate, taking into account the surface oxygen content of 8.9 at%, there can be about 255 such pairs of COO^- groups for a 5-nm particle, and the particle can potentially bind up to two hundred copper atoms. It follows from the EDX measurements that only 33 copper atoms are located on the particle surface. This value is close to the data (~20 Cu^{2+} ions per particle) obtained by the EPR method for the NDCu-iii sample, but, as in the case of XPS spectroscopy, the EDX method gives values exceeding those obtained using the EPR. This is understandable, since the EPR method observes copper only in the charge state Cu^{2+} and does not observe it in other states, for example, in the form of Cu^{1+} or neutral clusters.

It is very interesting that the supersaturation of the DND surface with metals (at density > 1.5 atoms nm^{-2}) most likely leads to the formation of scattered clusters of several tens of metal atoms or clusters of greater length on the particle surface. Such formations in the case of DND particles with an sp^2 graphene-like shell or material treatment in a reducing medium were observed for copper and palladium in the refs. 42–44. In the case of palladium on DND, the former can be used as an effective catalyst for a number of specific reactions.[42,43]

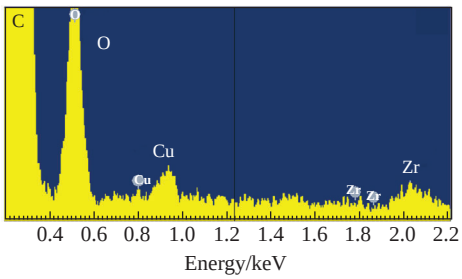

Figure 12 The EDX spectra of sample NDCu-iii taken from one of the local areas with a size of 100 × 100 microns, presented in an enlarged form in the energy range up to 2.2 keV. Copper and zirconium signals are clearly visible on the panel. The copper content is 0.29 at%. Other elements: C – 90.10 at%, O – 9.38 at%, Zr – 0.24 at%.

Other types of DND surface

It should also be noted that metal ions, for example, copper, can bind not only to the carboxylated, but also to the hydrogenated surface of DND particles *via* non-chelate mechanisms through substitutional nitrogen atoms located in the subsurface region.[29] The latter can act as electron acceptors and donors when interacting with surface agents (copper atoms and other entities). The binding energy of copper atoms with the surface in this case is very small. Such a surface should facilitate easy coalescence of copper atoms into clusters of several atoms.

Conclusion

The main outcome of the theoretical work preceding the recent experimental studies mainly done after 2015 was the demonstration of capability of DFT computations for adequate description of all stages of grafting the copper atoms on the surface of carboxylated nanodiamonds. Using the non-restricted approach extends the number of analysable structures. Totally this research opens the door for more detailed theoretical investigations of these more complexly modified nanoparticles.

The carboxylated surface of diamond is excellent for binding the cations of the 3*d*- and 4*f*-transition metals through the formation of chelate complexes. Using copper and gadolinium ions as an example, it is shown that magnetic methods can be successfully used to identify chelate complexes of 3*d* and 4*f* metals on the surface of DND particles. Magnetochemical methods make it possible to determine the concentration of metal ions with high accuracy, and the broadening of the main EPR signal of DND can also be used to analyze the proximity of the location of the magnetic moments of transition metals with respect to the paramagnetic spins and dangling bonds of DND particles. The maximum number of metal ions forming chelate complexes on the DND surface is ~8.7×10^{19} g^{-1} (or ~1700 ppm), which is associated with a limited number of chemically active sites (up to ~20 per particle) suitable for cation binding. At the same time, a larger number of copper atoms can be located on the surface or even in the space between particles in the form of neutral clusters of several atoms.

DND particles can be considered as a carrier of isolated copper ions for a wide range of tasks: from catalysis to the creation of composite polymer materials with a filler that has an antibacterial effect, which acts by slow elution of ionic copper as the polymer surface wears out.

V. O. acknowledges the support of the Russian Foundation for Basic Research (project no. 18-29-19038 мк) and is very grateful to Ms. Inna Suvorkova, Ms. Ekaterina Osipova, Dr. Nikolai Romanov, Dr. Yasushi Ishiguro and Prof. Kazuyuki Takai for help with sample characterization and cooperation.

Online Supplementary Materials

Supplementary data associated with this article can be found in the online version at doi: 10.1016/j.mencom.2022.03.001.

References

1 M. Baidakova and A. Vul', *J. Phys. D: Appl. Phys.*, 2007, **40**, 6300.
2 V. N. Mochalin, O. Shenderova, D. Ho and Y. Gogotsi, *Nat. Nanotechnol.*, 2012, **7**, 11.
3 V. Yu. Dolmatov, A. N. Ozerin, I. I. Kulakova, O. O. Bochechka, N. M. Lapchuk, V. Myllymäki and A. Vehanen, *Russ. Chem. Rev.*, 2020, **89**, 1428.
4 A. I. Shames, V. Yu. Osipov and A. M. Panich, *Phys. Chem. Chem. Phys.*, 2018, **20**, 27694.
5 V. Y. Dolmatov, V. Myllymäki and A. Vehanen, *J. Superhard Mater.*, 2013, **35**, 143.
6 V. Yu. Dolmatov, *Russ. Chem. Rev.*, 2007, **76**, 339 (*Usp. Khim.*, 2007, **76**, 375).

7 I. A. Rubtsov, *PhD Thesis*, Lavrentyev Institute of Hydrodynamics, Novosibirsk, 2021 (in Russian).
8 A. I. Shames, A. M. Panich, W. A. Kempiński, A. E. Alexenskii, M. V. Baidakova, A. T. Dideikin, V. Yu. Osipov, V. I. Siklitski, E. Osawa, M. Ozawa and A. Ya. Vul', *J. Phys. Chem. Solids*, 2002, **63**, 1993.
9 J. C. Arnault, in *Novel Aspects of Diamond: From Growth to Applications*, ed. N. Yang, Springer, 2015, pp. 85–122.
10 A. M. Schrand, S. A. Ciftan Hens and O. A. Shenderova, *Crit. Rev. Solid State Mater. Sci*., 2009, **34**, 18.
11 M. Chen, E. D. Pierstorff, R. Lam, S. Y. Li, H. Huang, E. Osawa and D. Ho, *ACS Nano*, 2009, **3**, 2016.
12 H. Huang, E. Pierstorff, E. Osawa and D. Ho, *Nano Lett.*, 2007, **7**, 3305.
13 K. Yano, T. Matsumoto, Y. Okamoto, K. Bito, N. Kurokawa, T. Hasebe and A. Hotta, *ACS Appl. Nano Mater.*, 2021, **4**, 1702.
14 A. M. Panich, M. Salti, S. D. Goren, E. B. Yudina, A. E. Aleksenskii, A. Ya. Vul' and A. I. Shames, *J. Phys. Chem. C*, 2019, **123**, 2627.
15 L. M. Manus, D. J. Mastarone, E. A. Waters, X. Q. Zhang, E. A. Shultz-Sikma, K. W. Machenaris, D. Ho and T. J. Meade, *Nano Lett.*, 2010, **10**, 484.
16 A. M. Panich, A. I. Shames, O. Medvedev, V. Yu. Osipov, A. E. Aleksenskiy and A.Ya. Vul', *Appl. Magn. Reson.*, 2009, **36**, 317.
17 A. I. Shames, A. M. Panich, V. Yu. Osipov, A. E. Aleksenskiy, A. Ya. Vul', T. Enoki and K. Takai, *J. Appl. Phys.*, 2010, **107**, 014318.
18 R. Kumar, S. Obrai, J. Mitra and A. Sharma, *Spectrochim. Acta, Part A*, 2013, **115**, 244.
19 M. Pavelka, M. Šimánek, J. Šponer and J. V. Burda, *J. Phys. Chem. A*, 2006, **110**, 4795.
20 P. Comba and M. Kerschner, *Coord. Chem. Rev*., 2009, **253**, 564 and references therein.
21 I. D. Gridnev, V. Yu. Osipov, A. E. Aleksenskii, A. Ya. Vul' and T. Enoki, *Bull. Chem. Soc. Jpn.*, 2014, **87**, 693.
22 V. Yu. Osipov, I. D. Gridnev and A. M. Panich, *Mendeleev Commun.*, 2018, **28**, 404.
23 E. B. Yudina, A. E. Aleksenskii, I. G. Fomina, A. V. Shvidchenko, D. P. Danilovich, I. L. Eremenko and A. Ya. Vul, *Eur. J. Inorg. Chem.*, 2019, **39**–**40**, 4345.
24 V. Yu. Osipov, A. E. Aleksenskiy, K. Takai and A. Y. Vul', *Phys. Solid State*, 2015, **57**, 2314 (*Fiz. Tverd. Tela*, 2015, **57**, 2245).
25 V. Yu. Osipov, N. M. Romanov, K. V. Bogdanov, F. Treussart, C. Jentgens and A. Rampersaud, *J. Opt. Technol*., 2018, **85**, 63 [*Opt. Zh.*, 2018, **85** (2), 3].
26 V. Yu. Osipov, D. W. Boukhvalov and K. Takai, *Mendeleev Commun*., 2020, **30**, 436.
27 K. Yano, T. Matsumoto, Y. Okamoto, K. Bito, N. Kurokawa, T. Hasebe and A. Hotta, *ACS Appl. Nano Mater.*, 2021, **4**, 1702.
28 A. M. Panich, M. Salti, O. Prager, E. Swissa, Y. V. Kulvelis, E. B. Yudina, A. E. Aleksenskii, S. D. Goren, A. Ya. Vul' and A. I. Shames, *Magn. Reson. Med.*, 2021, **86**, 935.
29 V. Yu. Osipov, D. W. Boukhvalov and K. Takai, *Mendeleev Commun*., 2019, **29**, 452.
30 A. I. Shames, V. Yu. Osipov, A. E. Aleksenskiy, E. Osawa and A. Ya. Vul', *Diamond Relat. Mater*., 2011, **20**, 318.
31 V. Yu. Osipov, N. M. Romanov, I. E. Suvorkova, E. V. Osipova, T. Tsuji, Y. Ishiguro and K. Takai, *Mendeleev Commun.*, 2022, **32**, 132.
32 N. Kobayashi, T. Enoki, C. Ishii, K. Kaneko and M. Endo, *J. Chem. Phys.*, 1998, **109**, 1983.
33 C. P. Slichter, *Principles of Magnetic Resonance*, Harper and Row, New York, 1963.
34 A. M. Panich, N. A. Sergeev and S. D. Goren, *Solid State Nucl. Magn. Reson*., 2020, **105**, 101624.
35 D. C. Frost, A. Ishitani and C. A. McDowell, *Mol. Phys.*, 1972, **24**, 861.
36 N. T. Bui, H. Kang, S. J. Teat, G. M. Su, C.-W. Pao, Y.-S. Liu, E. W. Zaia, J. Guo, J.-L. Chen, K. R. Meihaus, C. Dun, T. M. Mattox, J. R. Long, P. Fiske, R. Kostecki and J. J. Urban, *Nat. Commun*., 2020, **11**, 3947.
37 P. V. F. de Sousa, A. F. de Oliveira, A. A. da Silva and R. P. Lopes, *Environ. Sci. Pollut. Res. Int.*, 2019, **26**, 14883.
38 V. Yu. Osipov, N. M. Romanov, F. M. Shakhov and K. Takai, *J. Opt. Technol.*, 2018, **85**, 122 [*Opt. Zh*., 2018, **85** (3), 3].
39 A. E. Aleksenskii, V. Yu. Osipov, A. Ya. Vul', B. Ya. Ber, A. B. Smirnov, V. G. Melekhin, G. J. Adriaenssens and K. Iakoubovskii, *Phys. Solid State*, 2001, **43**, 145 (*Fiz. Tverd. Tela*, 2001, **43**, 140).
40 V. Yu. Osipov, F. Treussart, S. A. Zargaleh, K. Takai, F. M. Shakhov, B. T. Hogan and A. Baldycheva, *Nanoscale Res. Lett.*, 2019, **14**, 279.
41 J. Chastain and R. C. King, Jr., *Handbook of X-ray Photoelectron Spectroscopy*, Perkin-Elmer, Eden Prairie, MN, 1992.
42 O. V. Turova, E. V. Starodubtseva, M. G. Vinogradov, V. I. Sokolov, N. V. Abramova, A. Ya. Vul' and A. E. Alexenskiy, *Catal. Commun*., 2011, **12**, 577.
43 L. Zhang, H. Liu, X. Huang, X. Sun, Z. Jiang, R. Schlögl and D. Su, *Angew. Chem.*, 2015, **127**, 16049.
44 K. Turcheniuk and V. N. Mochalin, *Carbon*, 2016, **109**, 98.

Received: 27th October 2021; Com. 21/6741